Conceptual design of reinforced concrete structures using topology optimization with elasto-plastic material modeling

Michael Bogomolny and Oded Amir

Abstract Design of reinforced concrete structures is governed by the nonlinear behavior of concrete and by its different strengths in tension and compression. The purpose of this article is to present a computational procedure for optimal conceptual design of reinforced concrete structures, based on topology optimization with elasto-plastic material modeling. Concrete and steel are both considered as elasto-plastic materials, including the appropriate yield criteria and post-yielding response. The same approach can be applied also for topology optimization of other material compositions where nonlinear response must be considered. Optimized distribution of material is achieved by introducing interpolation rules for both elastic and plastic material properties. Several numerical examples illustrate the capability and potential of the proposed procedure.

Keywords Topology design, Plasticity, Reinforced concrete, Optimization

1 Introduction

Structural optimization techniques are now becoming an integral part of the design process and are widely applied, for example, in the automotive and aerospace industries. So far, optimal design had less impact on traditional structural engineering as practiced in the construction industry. One reason might be the difficulty in combining numerical optimization tools with models that can accurately represent the complex behavior of composite materials used by the building industry, such as reinforced concrete. The aim of this article is to present a computational procedure that enables optimal design of reinforced concrete structures. The approach can easily be generalized to accommodate other combinations of materials besides steel and concrete. By combining topology optimization with elasto-plastic modeling of the candidate materials, it is possible to consider not only the different elastic stiffnesses of the candidate materials, but also their distinct yield limits and yield criteria.

The main challenge in the design of structural elements made of reinforced concrete (RC) lies in the different strengths of concrete in tension and compression. Typical concrete mixes have high resistance to compressive stresses but due to the quasi-brittle nature, any appreciable tension (e.g. due to bending) will cause fracture and lead to failure of the structural element. Numerical analysis of RC structures is typically based on the finite element method. Since concrete itself is a composition of several materials, developing appropriate computational models is challenging and both nonlinear stress-strain relationship, as well as deformation localization effects are important. In practice, traditional

plasticity formulations constitute reasonable approximations to the underlying fracturing process. A key element in plasticity formulations is the yield or failure criteria. Several yield criteria have been applied in computational models for concrete. Early studies suggest using the Mohr-Coulomb or Drucker-Prager yield surfaces [9]. Aiming at formulating computational approaches that can match available experimental results, more advanced yield functions and plasticity formulations have been suggested over the years, for example by Lubliner et al. [16], Feenstra and de Borst [12], Pravida and Wunderlich [22] and Oliver et al. [21].

In practical design, RC members are treated as composite structures, where reinforcing steel bars are located in regions where tension (i.e. failure of plain concrete) is expected. Traditional methods may be sufficient for effectively distributing steel bars in standard structural elements such as beams, columns and slabs. However, nowadays advanced concrete technology - resulting in new and improved material properties - as well as new production methods, allow production of concrete structures of almost any shape, giving new freedom to the structural designer [20, 27]. This opens much room for applying structural optimization techniques, aimed at finding both the optimal shape of the concrete element as well as the optimal placement of reinforcement.

Up to date, the vast majority of studies in structural topology optimization were restricted to elastic material models (see Bendsøe and Sigmund [4] for a comprehensive review of the field). Elastic modeling is sufficient for determining the distribution of one or more material phases in a given domain, but only as long as all material points remain in their elastic stress state. This is clearly not the case in reinforced concrete, where the concrete phase fails under relatively low tension stresses. Therefore nonlinear material modeling is necessary when aiming at optimal design of RC structures. Several studies were dedicated to topology optimization of elasto-plastic structures, for example based on the von Mises yield criterion [29, 18] or the Drucker-Prager yield criterion [29]. However, to the best of the authors' knowledge, this is the first study where more than one nonlinear candidate material is considered. Lately, multiphase material optimization was utilized for improving the performance of fiber reinforced concrete [13]. Failure behavior of all candidate materials was considered, but the approach taken is restricted to layered structures and cannot provide general layouts as obtained using topology optimization.

One approach to visualizing the internal forces in cracked concrete beams is by a simple truss model introduced by Ritter [23]. The resulting model, widely known as the strut-and-tie model, has numerous applications in analysis and design of RC structures subjected to shear forces or torsion moments (e.g. Schlaich et al. [24], Marti [17]). Several researchers proposed to use a truss-like structure resulting from linear elastic topology optimization in order to predict a strut-and-tie model (Bruggi [6], Liang et al. [15] and Kwak and Noh [14]). Accordingly, the truss bars under tension forces represent the location of steel reinforcement while the compressed bars represent concrete. In the current study material nonlinearity of both concrete and steel is considered , and hence a more realistic model is obtained. An interpolation scheme is proposed, such that by changing the density (design variable of the optimization problem), the material properties and the failure criteria vary between concrete and steel. The result of the optimization process is the optimal distribution of concrete and steel inside a certain domain. Therefore an efficient strut-and-tie model is directly obtained.

The article is organized as follows: topology optimization is shortly introduced in Section 2, with emphasis on reinforcement design. The elasto-plastic models used for concrete and steel and the nonlinear finite element analysis are discussed in Section 3.

Section 4 is the heart of this article, where we present the material interpolation, the optimization problem formulation and the sensitivity analysis. Several demonstrative examples are presented in Section 5 and some conclusions are drawn in Section 6.

2 Design of linear elastic reinforcement using topology optimization

In this section, we shortly review topology optimization procedures, with particular emphasis on optimal layouts consisting of two materials, see Bendsøe and Sigmund [4] for an extensive report on topology optimization. We follow the material distribution approach for topological design [3] together with the SIMP (Solid Isotropic Material with Penalization) interpolation scheme [2]. The optimization problem aimed at finding the stiffest structural layout, usually known as the minimum compliance problem, is defined as follows

$$\begin{aligned} \min_{\boldsymbol{\rho}} c(\boldsymbol{\rho}) &= \mathbf{f}^T\mathbf{u} \\ \text{s.t.:} \quad & \sum_{e=1}^{N_e} v_e\rho_e \leq V \\ & 0 \leq \rho_e \leq 1 \qquad e = 1, ..., N_e \\ \text{with:} \quad & \mathbf{K}(\boldsymbol{\rho})\mathbf{u} = \mathbf{f} \end{aligned} \tag{1}$$

where $\mathbf{f}$ is the external load vector, $\mathbf{u}$ is the displacements vector, v_e is the element volume, ρ_e is the element density, V is the total available volume and $\mathbf{K}(\boldsymbol{\rho})$ is the stiffness matrix corresponding to the element densities $\boldsymbol{\rho}$

$$\mathbf{K}(\boldsymbol{\rho}) = \sum_{e=1}^{N_e}(E_{min} + (E_{max} - E_{min})\rho_e^{p_E})\mathbf{K}_e$$

In general, E_{min} and E_{max} are the values of Young's modulus corresponding to two candidate materials which should be distributed in the design domain. For the case of distributing a single material and void, E_{min} is set to a small positive value and E_{max} is typically set to 1. $\mathbf{K}_e$ represents the element stiffness matrix corresponding to the Young's modulus value of 1 and p_E is a penalization factor required to drive the design towards a 0-1 (or black and white) layout. For the purpose of clarity, filtering is not considered in the above formulation. Nevertheless, in many cases it is necessary to apply a filter in order to avoid checkerboard patterns and to obtain mesh-independent results [4].

In Figure 1, an optimized design obtained for a single linear elastic material (E_{min} represents void) is presented. The design domain is a rectangular simply supported beam; 25% of the total volume is available; and the load consists of a single point load. The obtained layout is a typical result of single-material topology optimization: the layouts usually resemble a truss/frame structure formed of several triangles. When E_{min} and E_{max} represent two materials (E_{min} is one order smaller than E_{max}), a different layout is obtained, see Figure 2. Such designs are typical for sandwich structures, consisting of a soft core and stiff sheets.

The optimized topologies obtained with linear elastic material modeling cannot be used directly in some design problems involving the composition of two materials. A

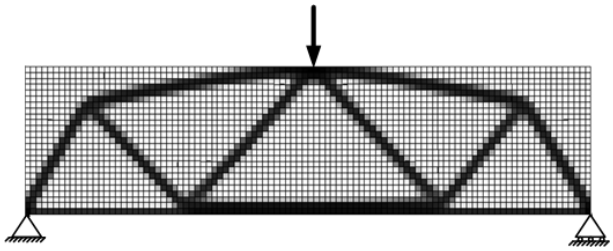

Figure 1: Optimized layout of a simply supported beam. Black: material, white: void.

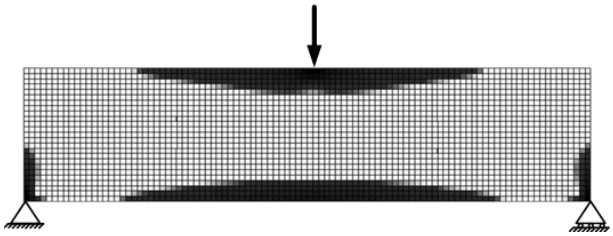

Figure 2: Optimized layout of a simply supported beam. Black: stiff material, white: soft material.

fundamental example is the design of reinforced concrete, where the design philosophy is based mainly on the fact that plain concrete has higher strength in compression than in tension, a property that is not captured by linear elastic modeling. In traditional reinforced concrete design, steel bars are positioned where tension stresses are expected. Therefore nonlinear material modeling is an essential component in optimal design of reinforced concrete and other compositions of materials with different nonlinear properties, taking into account not only the elastic stiffnesses of the two materials but also their yield limits and post-yielding behavior.

3 Nonlinear material model and finite element analysis

In this section, we shortly review the elasto-plastic model utilized in our study and outline the resulting nonlinear finite element problem to be solved. Later, in Section 4, the connection between the topology optimization problem and the nonlinear material model will be made.

3.1 Elasto-plastic material model

The main purpose of this study is to optimize the distribution of two materials in a given domain, taking the different nonlinear behavior of both materials into account. The main idea is to represent the elasto-plastic response of both materials using one generic yield function that varies according to the value of the design variable. For this purpose, we utilize the Drucker-Prager yield criterion [11]. For certain choices of material properties, the Drucker-Prager yield function can model the behavior of materials that are much stronger in compression than in tension, such as soils, rock or plain concrete. Moreover,

the von Mises yield criterion which is widely used for metals (having equal strength in tension and compression) can be seen as a particular case of the Drucker-Prager criterion.

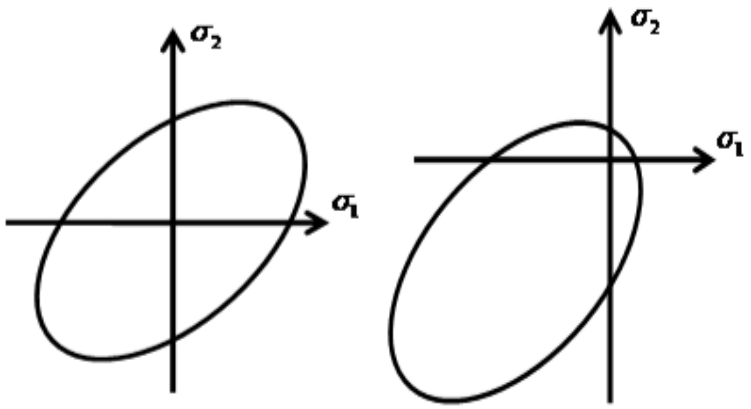

(a) von Mises (b) Drucker-Prager

Figure 3: Yield surfaces in 2D principal stress space.

As a demonstrative case we focus throughout this article on the distribution of concrete and steel. In essence, the purpose of utilizing nonlinear modeling is to identify the failure of concrete when tension stresses appear and then redistribute material so that such failure does not occur. Other aspects of the elasto-plastic behavior, namely yielding of steel in both stress states or yielding of concrete in compression, are categorized as less important for the purpose of this study. Therefore some simplifying assumptions are made in the formulation of the nonlinear material model, which would not be allowed if the purpose was accurate prediction of failure and damage in reinforced concrete structures.

In the following, we present the governing equations of the elasto-plastic model, leading to the local constitutive problem to be solved on a Gauss-point level. We follow classical rate-independent plasticity formulations, based on the textbooks by Simo and Hughes [26] and Zienkiewicz and Taylor [30]. The Drucker-Prager yield function can be expressed as

$$f(\boldsymbol{\sigma}, \kappa) = \sqrt{3J_2} + \alpha(\kappa) I_1 - \sigma_y(\kappa) \leq 0$$

where J_2 is the second invariant of the deviatoric stress tensor and I_1 is the first invariant (trace) of the stress tensor. α is a material property and σ_y is the yield stress in uniaxial tension, both functions of the internal hardening parameter κ according to some hardening functions. The expression $\sqrt{3J_2}$ is usually known as the *von Mises stress* or *equivalent stress*. When $\alpha = 0$, we obtain the von Mises yield criterion. We assume simple isotropic hardening rules

$$\alpha(\kappa) = constant \tag{2}$$

$$\sigma_y(\kappa) = \sigma_y^0 + HE\kappa \tag{3}$$

where σ_y^0 is the initial uniaxial yield stress, E is Young's modulus and H is a constant, typically in the order of 10^{-2}. The assumptions (2) and (3) are not necessarily suitable for accurate modeling of concrete but do not affect the ability to capture the most important failure in concrete, that is failure in tension. We assume an associative flow rule and a

simple relation between the hardening parameter and the rate of the plastic flow

$$\begin{aligned} \dot{\boldsymbol{\epsilon}}^{pl} &= \dot{\lambda}\frac{\partial f}{\partial \boldsymbol{\sigma}} \\ \dot{\kappa} &= \dot{\lambda} \end{aligned} \tag{4}$$

where $\boldsymbol{\epsilon}^{pl}$ is the plastic strain tensor and the scalar λ is usually referred to as the *plastic multiplier*. The relation (4) does not accurately represent hardening mechanisms in metals. Nevertheless, it is accurate enough for the purpose of the current study, since post-yielding response of the steel phase should not have an effect on the optimal choice of material. Together with the yield criterion, $\dot{\lambda}$ must satisfy the Kuhn-Tucker complementarity conditions

$$\begin{aligned} \dot{\lambda} &\geq 0 \\ f(\boldsymbol{\sigma}, \kappa) &\leq 0 \\ \dot{\lambda} f(\boldsymbol{\sigma}, \kappa) &= 0 \end{aligned}$$

The continuum problem (in the temporal sense) is transformed into a discrete constrained optimization problem by applying an implicit backward-Euler difference scheme. The central feature of this scheme is the introduction of a trial elastic state. For any given incremental displacement field, it is first assumed that there is no plastic flow between time t_n and the next time step t_{n+1}, meaning the incremental elastic strains are the incremental total strains. It can be shown that the the loading/unloading situation which is governed by the Kuhn-Tucker conditions can be identified using the trial elastic state [26]. Once a plastic increment occurs, the new state variables can be found by solving a nonlinear equation system resulting from the time discretization of the governing equations. For the current model, the derivation of the discrete equation system is as follows. The total strain is split into its elastic and plastic parts

$$\boldsymbol{\epsilon} = \boldsymbol{\epsilon}^{el} + \boldsymbol{\epsilon}^{pl}$$

The stress rate is related to the elastic strain rate via the elastic constitutive tensor $\mathbf{D}$

$$\dot{\boldsymbol{\sigma}} = \mathbf{D}\dot{\boldsymbol{\epsilon}}^{el}$$

So for a certain "time" increment we can write the linearized equation

$$\Delta\boldsymbol{\sigma} = \mathbf{D}(\Delta\boldsymbol{\epsilon} - \Delta\boldsymbol{\epsilon}^{pl}) = \mathbf{D}(\Delta\boldsymbol{\epsilon} - \Delta\lambda\frac{\partial f}{\partial \boldsymbol{\sigma}})$$

Multiplying by $\mathbf{D}^{-1}$ leads to the first set of equations to be solved

$$\Delta\boldsymbol{\epsilon} - \mathbf{D}^{-1}\Delta\boldsymbol{\sigma} - \frac{\partial f}{\partial \boldsymbol{\sigma}}\Delta\lambda = \mathbf{0} \tag{5}$$

An additional equation results from the requirement that after initial yielding, the stress state should satisfy the yield condition

$$f(\boldsymbol{\sigma}, \lambda) = \sqrt{3J_2} + \alpha I_1 - \sigma_y(\lambda) = 0 \tag{6}$$

3.2 Nonlinear finite element analysis

Throughout this study, we follow the framework described by Michaleris et al. [19] for nonlinear finite element analysis and adjoint sensitivity analysis, where the elasto-plastic nonlinear analysis is seen as a transient, nonlinear coupled problem. In the coupled approach, for every increment n in the transient analysis, we determine the unknowns $\mathbf{u}_n$ (displacements) and $\mathbf{v}_n$ (stresses and plastic multipliers) that satisfy the residual equations

$$\begin{aligned} \mathbf{R}_n(\mathbf{u}_n, \mathbf{u}_{n-1}, \mathbf{v}_n, \mathbf{v}_{n-1}) &= 0 \\ \mathbf{H}_n(\mathbf{u}_n, \mathbf{u}_{n-1}, \mathbf{v}_n, \mathbf{v}_{n-1}) &= 0 \end{aligned} \tag{7}$$

where $\mathbf{R}_n = 0$ is satisfied at the global level and $\mathbf{H}_n = 0$ is satisfied at each Gauss point. The transient, coupled and nonlinear system of equations is uncoupled by treating the response $\mathbf{v}$ as a function of the response $\mathbf{u}$. When solving the residual equations for the n-th "time" increment, the responses $\mathbf{u}_{n-1}$ and $\mathbf{v}_{n-1}$ are known from the previous converged increment. The independent response $\mathbf{u}_n$ is found by an iterative prediction-correction procedure in the global level, while for each iterative step the dependent response $\mathbf{v}_n(\mathbf{u}_n)$ is found by an inner iterative loop. The responses $\mathbf{u}_n$ and its dependant $\mathbf{v}_n$ are corrected until Eq. (7) is satisfied to sufficient accuracy. This procedure is repeated for all N increments.

Neglecting body forces, $\mathbf{R}_n$ is defined as the difference between external and internal forces and depends explicitly only on $\mathbf{v}_n$

$$\mathbf{R}_n(\mathbf{v}_n) = \mathbf{f}_n - \int_V \mathbf{B}^T \boldsymbol{\sigma}_n dV$$

where $\mathbf{B}$ is the standard strain-displacement matrix in the context of finite element procedures. The internal, Gauss-point level variables $\mathbf{v}_n$ are defined as

$$\mathbf{v}_n = \begin{bmatrix} \boldsymbol{\sigma}_n \\ \lambda_n \end{bmatrix}$$

where $\boldsymbol{\sigma}_n$ are the stresses and λ_n is the plastic multiplier. Furthermore, the residual $\mathbf{H}_n$ is defined as the collection of two incremental residuals, resulting from Eqs. (5),(6)

$$\mathbf{H}_n(\mathbf{u}_n, \mathbf{u}_{n-1}, \mathbf{v}_n, \mathbf{v}_{n-1}) = \begin{bmatrix} \mathbf{B}\mathbf{u}_n - \mathbf{B}\mathbf{u}_{n-1} - \mathbf{D}^{-1}(\boldsymbol{\sigma}_n - \boldsymbol{\sigma}_{n-1}) - \frac{\partial f}{\partial \boldsymbol{\sigma}_n}(\lambda_n - \lambda_{n-1}) \\ \sqrt{3J_2} + \alpha I_1 - \sigma_y(\lambda_n) \end{bmatrix} = \mathbf{0} \tag{8}$$

Here, the first equation equates total, elastic and plastic strains and the second represents the requirement that during plastic response the stress state satisfies the yield condition. In case an elastic step is predicted by the trial state, then no plastic flow occurs and $\lambda_n = \lambda_{n-1}$. Therefore the first equation is satisfied trivially by the elastic stress-strain relationship and the second equation can be disregarded.

The elasto-plastic problem is path-dependent by nature, meaning that the evolution of plastic strains under a certain load intensity depends on the history of plastic straining and cannot be computed correctly in one load stage. In practice, this means that the FE analysis must be solved incrementally. The default choice for most nonlinear FE solvers is to use *load control*, meaning that the total load is divided into a certain number of increments. Then for each increment, the current stress and strain states are required for the solution of the local elasto-plastic problem corresponding to the next load step. In some cases it is beneficial to switch to *displacement control*, for example when a small

addition to the load causes a large additional displacement or when limit points are encountered [10]. In the context of optimal design, a fixed load intensity throughout the optimization process may cause difficulties in solving the nonlinear analysis equations for intermediate designs that are very flexible. From this point of view, using displacement control for the nonlinear analysis is preferable. This means that the displacement at a selected degree of freedom is prescribed to a certain value for all design cycles. Choosing an appropriate value is possible if the designer has some knowledge regarding the expected deformation, and can also be seen as a way of imposing a required deflection at a certain point. Displacement control was utilized also in previous studies regarding topology optimization of elasto-plastic structures, e.g. by Swan and Kosaka [29] and Maute et al. [18].

For these reasons we mainly use displacement control and corresponding objective functions in this study. Then the global residual equation (7) takes the form

$$\mathbf{R}_n(\mathbf{v}_n, \theta_n) = \theta_n \hat{\mathbf{f}} - \int_V \mathbf{B}^T \boldsymbol{\sigma}_n dV$$

where θ_n is the (unknown) load factor in the n-th increment and $\hat{\mathbf{f}}$ is a constant reference load vector with non-zero entries only at loaded degrees of freedom. When solving the coupled equation system for each increment, a single displacement has a prescribed value and the rest, as well as the corresponding load factor θ_n, are determined from equilibrium.

4 Problem formulation

4.1 Interpolation of material properties

The main idea is to interpolate the nonlinear behavior of the two candidate materials using the density variables from the topology optimization problem. The interpolation of the elastic modulus is identical to that used in standard, linear elastic topology optimization

$$E(\rho_e) = E_{min} + (E_{max} - E_{min})\rho_e^{p_E} \tag{9}$$

where ρ_e is the density design variable corresponding to a certain finite element e. Interpolation of the nonlinear response is achieved by adding a dependency on the design variable ρ to the yield function, so instead of Eq. (6) we have

$$f(\boldsymbol{\sigma}, \lambda, \rho_e) = \sqrt{3J_2} + \alpha(\rho_e) I_1 - \sigma_y(\lambda, \rho_e) = 0 \tag{10}$$

Following a SIMP-type approach, the interpolating functions $\alpha(\rho_e)$ and $\sigma_y(\rho_e)$ are given by

$$\alpha(\rho_e) = \alpha_{max} - (\alpha_{max} - \alpha_{min})\rho_e^{p_\alpha} \tag{11}$$

$$\sigma_y(\lambda, \rho_e) = \sigma^0_{y,min} + (\sigma^0_{y,max} - \sigma^0_{y,min})\rho_e^{p_{\sigma_y}} + HE(\rho_e)\lambda \tag{12}$$

where p_α and p_{σ_y} are penalization factors for α and σ_y, respectively. These interpolations imply that the yield surface of one material is obtained by choosing $\rho_e = 0$, meaning $\alpha = \alpha_{max}$ and $\sigma^0_y = \sigma^0_{y,min}$, and the second yield surface is obtained by $\rho_e = 1$, meaning $\alpha = \alpha_{min}$ and $\sigma^0_y = \sigma^0_{y,max}$. As stated above, the particular case $\alpha_{min} = 0$ means that the plastic response of the second material is governed by the von Mises yield criterion. By setting also $\sigma^0_{y,max} = \sigma^0_{y,steel}$ an actual model of steel is obtained for $\rho_e = 1$. In Figure 4,

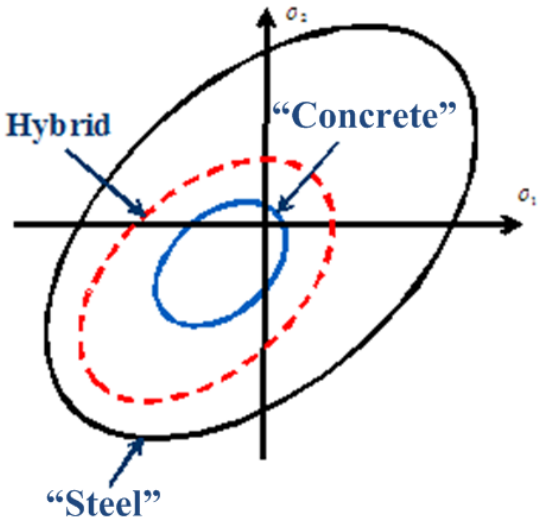

Figure 4: Demonstrative example of the interpolation between two yield surfaces, presented in 2D principal stress space. The "Hybrid" surface represents the behavior of an artificial mixture, corresponding to an intermediate density in topology optimization.

the interpolation of the yield surfaces is demonstrated, for two materials resembling steel and concrete.

In order to obtain optimized designs with general concrete topologies, we extend this interpolation so it accommodates also void regions. Following [25], we add another design variable x for each finite element. Void regions are represented by $x = 0$ and solid regions are represented by $x = 1$. Within the solid regions, the value of ρ determines the distribution of the two candidate materials. This leads to the following interpolation functions, replacing Eqs. (9), (10), (11), (12)

$$E(x_e, \rho_e) = x_e^{p_{Ex}}(E_{min} + (E_{max} - E_{min})\rho_e^{p_E}) \quad (13)$$

$$f(\boldsymbol{\sigma}, \lambda, \rho_e, x_e) = \sqrt{3J_2} + \alpha(x_e, \rho_e)I_1 - \sigma_y(\lambda, x_e, \rho_e) = 0 \quad (14)$$

$$\alpha(x_e, \rho_e) = x_e^{p_{\alpha x}}(\alpha_{max} - (\alpha_{max} - \alpha_{min})\rho_e^{p_\alpha}) \quad (15)$$

$$\sigma_y(\lambda, x_e, \rho_e) = x_e^{p_{\sigma x}}(\sigma^0_{y,min} + (\sigma^0_{y,max} - \sigma^0_{y,min})\rho_e^{p_{\sigma y}} + HE(x_e, \rho_e)\lambda) \quad (16)$$

where p_{Ex}, $p_{\alpha x}$ and $p_{\sigma x}$ are penalization factors for x. In practice, one may choose to use the same penalty factors for both design variables, x and ρ.

4.2 Optimization problem and sensitivity analysis

In this article, we focus mainly on one demonstrative class of objective functions. The aim is to find the stiffest structural layouts given certain amounts of available material. When only linear elastic response is considered, the corresponding objective is the widely used minimum compliance problem, presented above (1). When nonlinear response is taken into account, one may define several different objectives that are related to the maximization of the structural stiffness (see for example [29], [18], [8]). Since displacement control is preferred in the nonlinear FE analysis, a possible equivalent to minimizing compliance in linear elasticity is maximizing the end compliance for a given prescribed

displacement. In other words, the objective is to maximize the magnitude of the load that corresponds to a certain prescribed displacement at a particular degree of freedom.

Assuming the analysis problem is solved in N increments, the optimization problem of distributing two materials in the design domain can be stated as follows

$$\begin{aligned} \min_{\boldsymbol{\rho}} c(\boldsymbol{\rho}) &= -\theta_N \hat{\mathbf{f}}^T \mathbf{u}_N \\ \text{s.t.:} \quad & \sum_{e=1}^{N_e} v_e \rho_e \leq V \\ & 0 \leq \rho_e \leq 1, \qquad e = 1, ..., N_e \\ \text{with the coupled residuals:} \quad & \mathbf{R}_n(\mathbf{v}_n, \theta_n) = 0 \qquad n = 1, ..., N \\ & \mathbf{H}_n(\mathbf{u}_n, \mathbf{u}_{n-1}, \mathbf{v}_n, \mathbf{v}_{n-1}, \boldsymbol{\rho}) = 0 \qquad n = 1, ..., N \end{aligned} \tag{17}$$

where V is the available volume of the material whose properties correspond to $\rho_e = 1$. When distributing two materials and void, the optimization problem is slightly modified

$$\begin{aligned} \min_{\boldsymbol{\rho}, \mathbf{x}} c(\boldsymbol{\rho}, \mathbf{x}) &= -\theta_N \hat{\mathbf{f}}^T \mathbf{u}_N \\ \text{s.t.:} \quad & \sum_{e=1}^{N_e} v_e x_e \leq V_1 \\ & \sum_{e=1}^{N_e} v_e \rho_e \leq V_2 \\ & 0 < x_{min} \leq x_e \leq 1, \qquad e = 1, ..., N_e \\ & 0 \leq \rho_e \leq 1, \qquad e = 1, ..., N_e \\ \text{with the coupled residuals:} \quad & \mathbf{R}_n(\mathbf{v}_n, \theta_n) = 0 \qquad n = 1, ..., N \\ & \mathbf{H}_n(\mathbf{u}_n, \mathbf{u}_{n-1}, \mathbf{v}_n, \mathbf{v}_{n-1}, \boldsymbol{\rho}, \mathbf{x}) = 0 \qquad n = 1, ..., N \end{aligned} \tag{18}$$

where V_1 is the total available volume of material, V_2 is the available volume of the material whose properties correspond to $\rho_e = 1$ ($V_2 \leq V_1$) and x_{min} is a positive lower bound used in order to avoid singularity of the stiffness matrix.

As mentioned earlier, the design sensitivities are computed by the adjoint method, following the framework for transient, nonlinear coupled problems described by Michaleris et al. [19]. To the best of the authors' knowledge, this is the first implementation of this framework in topology optimization of structures with material nonlinearities. Furthermore, it is presumably the first sensitivity analysis for topology optimization of structures with material nonlinearities where no simplifying assumptions are made. An effort is made to use similar notation to that in [19]. The procedure for sensitivity analysis is described here only for the two material and void problem (18) since the two-material problem can easily be deduced from it. We begin by forming the augmented objective function $\hat{c}(\boldsymbol{\rho})$

$$\begin{aligned} \hat{c}(\boldsymbol{\rho}, \mathbf{x}) &= -\theta_N \hat{\mathbf{f}}^T \mathbf{u}_N - \sum_{n=1}^{N} \boldsymbol{\lambda}_n^T \mathbf{R}_n(\mathbf{v}_n, \theta_n) \\ & \quad - \sum_{n=1}^{N} \boldsymbol{\gamma}_n^T \mathbf{H}_n(\mathbf{u}_n, \mathbf{u}_{n-1}, \mathbf{v}_n, \mathbf{v}_{n-1}, \boldsymbol{\rho}, \mathbf{x}) \end{aligned}$$

where $\boldsymbol{\lambda}_n$ and $\boldsymbol{\gamma}_n$ are the adjoint vectors to be found for all increments $n = 1, ..., N$. We assume the initial responses $\mathbf{u}_0$, $\mathbf{v}_0$ do not depend on the design variables. Furthermore,

it can be observed that the objective function and the nonlinear equation systems $\mathbf{R}_n = 0$ $(n = 1, ..., N)$ do not depend explicitly on the design variables. Therefore the explicit terms in the derivative of the augmented objective with respect to the design variables are

$$\begin{aligned} \frac{\partial \hat{c}_{exp}}{\partial x_e} &= -\sum_{n=1}^{N} \boldsymbol{\gamma}_n^T \frac{\partial \mathbf{H}_n}{\partial x_e} \\ \frac{\partial \hat{c}_{exp}}{\partial \rho_e} &= -\sum_{n=1}^{N} \boldsymbol{\gamma}_n^T \frac{\partial \mathbf{H}_n}{\partial \rho_e} \end{aligned}$$

The adjoint vectors $\boldsymbol{\gamma}_n$ $(n = 1, ..., N)$ are computed on a Gauss-point level by a backward incremental procedure, which is required due to path dependency of the elasto-plastic response. The backward procedure consists of the collection of equation systems resulting from the requirement that all implicit derivatives of the design variables will vanish. Further details regarding the adjoint procedure can be found in [1]. For performing the backwards-incremental sensitivity analysis, the derivatives of the global and local residuals with respect to the analysis variables are required. These are given in this section for the elasto-plastic model utilized in the current study. In particular, we consider a plane stress situation, meaning the stresses and strains are collected in a vector with three entries: $\boldsymbol{\sigma} = [\sigma_{11}, \sigma_{22}, \sigma_{12}]^T$ and $\boldsymbol{\epsilon} = [\epsilon_{11}, \epsilon_{22}, \epsilon_{12}]^T$.

The derivative of the global residual is independent of the specific material model employed and is given by

$$\frac{\partial(\mathbf{R}_n)}{\partial(\mathbf{v}_n)} = \left[\begin{array}{cc} -\mathbf{B}^T w J_{(8\times3)} & \mathbf{0}_{(8\times1)} \end{array} \right]$$

where $\mathbf{B}$ is the standard strain-displacement matrix; w is the Gauss-point weight for numerical integration; and J is the determinant of the Jacobian at the Gauss-point. For the nonlinear material model described in Section 3, the derivatives of the local residual are

$$\begin{aligned} \frac{\partial(\mathbf{H}_n)}{\partial(\mathbf{u}_n)} &= \left[\begin{array}{c} \mathbf{B}_{(3\times8)} \\ \mathbf{0}_{(1\times8)} \end{array} \right] \\ \frac{\partial(\mathbf{H}_{n+1})}{\partial(\mathbf{u}_n)} &= \left[\begin{array}{c} -\mathbf{B}_{(3\times8)} \\ \mathbf{0}_{(1\times8)} \end{array} \right] \\ \frac{\partial(\mathbf{H}_n)}{\partial(\mathbf{v}_n)} &= \left[\begin{array}{cc} -\mathbf{D}^{-1} - \Delta^n \lambda \frac{\partial^2 f}{\partial \boldsymbol{\sigma}_n}_{(3\times3)} & -\frac{\partial f}{\partial \boldsymbol{\sigma}_n}^T_{(3\times1)} \\ \frac{\partial f}{\partial \boldsymbol{\sigma}_n}_{(1\times3)} & -HE_{(1\times1)} \end{array} \right] \\ \frac{\partial(\mathbf{H}_{n+1})}{\partial(\mathbf{v}_n)} &= \left[\begin{array}{cc} \mathbf{D}^{-1}{}_{(3\times3)} & \frac{\partial f}{\partial \boldsymbol{\sigma}_{n+1}}^T_{(3\times1)} \\ \mathbf{0}_{(1\times3)} & 0_{(1\times1)} \end{array} \right] \end{aligned}$$

where the derivative of the yield function with respect to the stress components is

$$\frac{\partial f}{\partial \boldsymbol{\sigma}} = \frac{1}{2\sqrt{3J_2}} \left[\begin{array}{ccc} 2\sigma_{11} - \sigma_{22} & 2\sigma_{22} - \sigma 11 & 6\sigma_{12} \end{array} \right] + \alpha \left[\begin{array}{ccc} 1 & 1 & 0 \end{array} \right]$$

In actual implementation, the derivatives of the local residuals $\mathbf{H}_n$ and $\mathbf{H}_{n+1}$ should maintain consistency with respect to the analysis. This means that some rows and columns

should be disregarded in case of elastic loading or unloading. For example, if increment n is elastic, then we have $\frac{\partial(\mathbf{H}_n)}{\partial(\mathbf{u}_n)} = \left[\mathbf{B}_{(3\times 8)}\right]$ and $\frac{\partial(\mathbf{H}_n)}{\partial(\mathbf{v}_n)} = \left[-\mathbf{D}^{-1}_{(3\times 3)}\right]$.

Finally, computing the derivatives $\frac{\partial \mathbf{H}_n}{\partial x_e}$, $\frac{\partial \mathbf{H}_n}{\partial \rho_e}$ requires adding the dependency on the design variables to Eq. (8) and differentiating with respect to x_e and ρ_e. This leads to

$$\begin{aligned}
\frac{\partial \mathbf{H}_n}{\partial x_e} &= \begin{bmatrix} -\frac{\partial(\mathbf{D}(x_e,\rho_e)^{-1})}{\partial x_e}(\boldsymbol{\sigma}_n - \boldsymbol{\sigma}_{n-1}) - \frac{\partial(\frac{\partial f}{\partial \boldsymbol{\sigma}_n}(x_e,\rho_e))^T}{\partial x_e}(\lambda_n - \lambda_{n-1}) \\ \frac{\partial f(x_e,\rho_e)}{\partial x_e} \end{bmatrix} \\
\frac{\partial \mathbf{H}_n}{\partial \rho_e} &= \begin{bmatrix} -\frac{\partial(\mathbf{D}(x_e,\rho_e)^{-1})}{\partial \rho_e}(\boldsymbol{\sigma}_n - \boldsymbol{\sigma}_{n-1}) - \frac{\partial(\frac{\partial f}{\partial \boldsymbol{\sigma}_n}(x_e,\rho_e))^T}{\partial \rho_e}(\lambda_n - \lambda_{n-1}) \\ \frac{\partial f(x_e,\rho_e)}{\partial \rho_e} \end{bmatrix}
\end{aligned}$$

where

$$\begin{aligned}
\frac{\partial(\mathbf{D}(x_e,\rho_e)^{-1})}{\partial x_e} &= -\frac{1}{E(x_e,\rho_e)}\frac{\partial E(x_e,\rho_e)}{\partial x_e}\mathbf{D}(x_e,\rho_e)^{-1} \\
\frac{\partial(\mathbf{D}(x_e,\rho_e)^{-1})}{\partial \rho_e} &= -\frac{1}{E(x_e,\rho_e)}\frac{\partial E(x_e,\rho_e)}{\partial \rho_e}\mathbf{D}(x_e,\rho_e)^{-1} \\
\frac{\partial(\frac{\partial f}{\partial \boldsymbol{\sigma}_n}(x_e,\rho_e))^T}{\partial x_e} &= \frac{\partial \alpha(x_e,\rho_e)}{\partial x_e}\begin{bmatrix} 1 \\ 1 \\ 0 \end{bmatrix} \\
\frac{\partial(\frac{\partial f}{\partial \boldsymbol{\sigma}_n}(x_e,\rho_e))^T}{\partial \rho_e} &= \frac{\partial \alpha(x_e,\rho_e)}{\partial \rho_e}\begin{bmatrix} 1 \\ 1 \\ 0 \end{bmatrix} \\
\frac{\partial f(x_e,\rho_e)}{\partial x_e} &= \frac{\partial \alpha(x_e,\rho_e)}{\partial x_e}I_1 - \frac{\partial \sigma_y(x_e,\rho_e)}{\partial x_e} \\
\frac{\partial f(x_e,\rho_e)}{\partial \rho_e} &= \frac{\partial \alpha(x_e,\rho_e)}{\partial \rho_e}I_1 - \frac{\partial \sigma_y(x_e,\rho_e)}{\partial \rho_e}
\end{aligned}$$

The above derivatives can be easily computed using the relations given in Eqs. (13), (14), (15), (16).

Remarks regarding sensitivity analysis for displacement-controlled analysis The objective function used in the problem formulations above is appropriate for stiffness maximization only in the case of a single point load. Applying a distributed load while prescribing a single displacement poses a problem when defining a proper objective for stiffness maximization. As discussed in [1], maximizing the global end-compliance $\theta\widehat{\mathbf{f}}_{ext}^T\mathbf{u}$ may result in a structure that is very stiff with respect to bearing the load at the prescribed DOF but very flexible with respect to all other loads. Therefore when a distributed load is applied, the objective is defined as minimizing the end-compliance ${\mathbf{f}_{ext}}^T\mathbf{u}$ *as if* the analysis is load-controlled and *as if* the load intensity is constant throughout the optimization. The resulting hybrid procedure combines the advantages of both load and displacement control. On the one hand, the analysis is more stable numerically and is more likely to converge when the structural layout is relatively "soft". On the other hand, the objective is well-defined and should lead to the best global stiffness with respect to all the applied loads. In practice, this can be seen as a load-controlled procedure, just that the load intensity varies throughout the design process to fit the prescribed displacement. Moreover, in the sensitivity analysis it is assumed that the solution was obtained using load control, which

leads to a more straightforward computational procedure. This procedure is demonstrated on a compliance objective in a single degree of freedom space in Figure 5. For comparison, the standard procedures for either load or displacement control are also sketched. It can be seen that the hybrid approach is equivalent to a load-controlled approach where the load intensity varies throughout the optimization process. In particular, the varying load level is determined implicitly by the displacement-controlled analysis.

5 Examples

In this section we present several results obtained when implementing the computational approach described in this article. The purpose is to demonstrate the capabilities and potential of our approach and to gain insight regarding implementation aspects. Therefore, as preliminary examples we consider relatively small scale two-dimensional problems with no self weight. Extending to three dimensional models and incorporating more realistic loading conditions are among the goals of future work.

5.1 General considerations

The examples presented refer to both the distribution of concrete and steel (17) as well as to the distribution of concrete, steel and void (18). The material parameters resemble actual values corresponding to steel and concrete, see Table 1. For computing α_{max} and $\sigma^0_{y,min}$, both corresponding to the concrete phase, it was assumed that the strength of concrete in compression is ten times higher than in tension. All test cases were solved using a 2D finite element mesh consisting of square, bi-linear plane stress elements. The optimization was performed by a nonlinear optimization program based on the Method of Moving Asymptotes - MMA [28]. In order to obtain regularized designs and to avoid checkerboard patterns, a density filter was applied [5, 7].

Table 1: Material properties in all test cases

Parameter	Material	Value
E_{min}	concrete	25.0 [GPa]
E_{max}	steel	200.0 [GPa]
α_{min}	steel	0.0
α_{max}	concrete	0.818
$\sigma^0_{y,min}$	concrete	5.5 [MPa]
$\sigma^0_{y,max}$	steel	300 [MPa]
ν	both	0.3
H	both	0.01

The actual computational performance of the proposed approach is affected by the choice of several numerical parameters. First, one should carefully choose an appropriate value of the prescribed displacement, denoted by δ. From the computational point of view, an appropriate value of δ is necessary in order to ensure convergence of the Newton-Raphson iterations in the nonlinear FE analysis. Too large values of δ may cause difficulties in convergence, thus increasing the computing time. At the same time, δ should

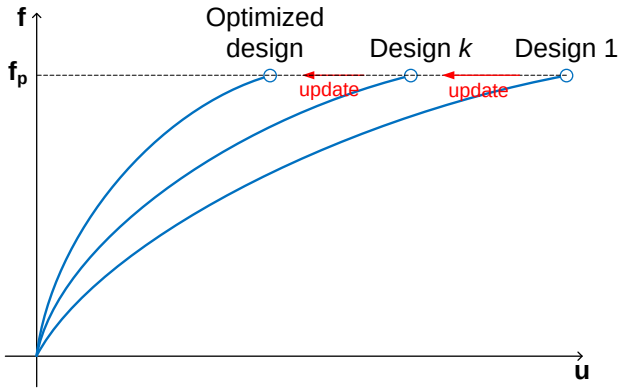

(a) Load-controlled setting

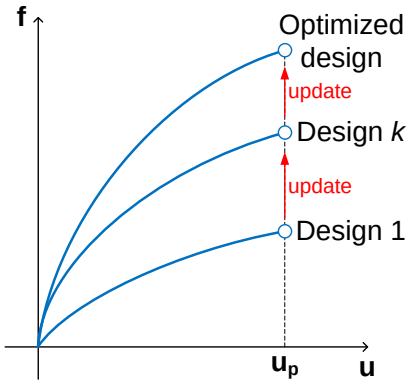

(b) Displacement-controlled setting

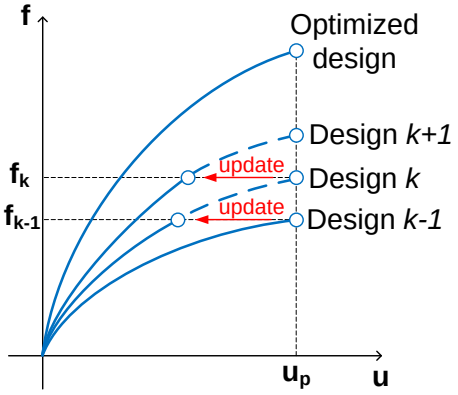

(c) Hybrid approach

Figure 5: Comparison of approaches for optimal design considering structural nonlinearities. In a load-controlled setting (top), the designs are evaluated at the same load level and updated accordingly. In a displacement-controlled setting (middle), the designs are evaluated at the same displacement level and updated accordingly. In the hybrid approach (bottom), each design is evaluated at the prescribed displacement level, but then updated according to the corresponding load level.

be large enough to ensure that the response of the structure is indeed nonlinear. From a practical point of view, δ should also fit realistic deflections of reinforced concrete structures. In the current implementation, in case the nonlinear analysis fails to converge at a certain displacement level even after several increment cuts, the analysis is terminated and sensitivity analysis is performed with respect to the converged configuration.

As for the optimization process, it is well known that in topology optimization the computational performance is strongly affected by the choice of the filter radius and penalty factors. An effort was made to keep these values similar for all test cases. In some cases, the penalty factors are gradually increased and/or the filter radius is gradually decreased in order to obtain a more refined layout. The particular choice of numerical parameters for each test case is given in the corresponding text. The number of design iterations varies between test cases. According to the authors' experience, most problems require 100 to 200 design iterations to reach a distinct layout. After that, no significant changes in the layout can be observed and the improvement in objective value is negligible. The relatively tight convergence tolerance (1×10^{-4}) referring to the maximum change in an element density throughout the design domain was not reached.

5.2 Optimized concrete-steel layouts

Example 1. Simply supported beam subject to a concentrated load In this example problem, the competence of the proposed procedure in designing the reinforcement for a simply supported beam is demonstrated. We consider a beam with a length-to-height ratio equal to 4, loaded with a prescribed displacement directed downwards at the middle of the top edge, see Figure 6. The model of the symmetric half is discretized with a 200×100 FE mesh. We first discuss the maximization of the end-compliance, see (17). We examine three volume fractions for the steel constituent: 0.05, 0.1 and 0.2 and the magnitude of the prescribed displacement δ is set to 0.001, 0.002 and 0.005 respectively. In some cases, the final design is achieved by gradually increasing all penalty factors and reducing the filter radius, for details see Table 2. This is necessary in order to remove "gray" regions of intermediate density, as well as small isolated reinforcement regions.

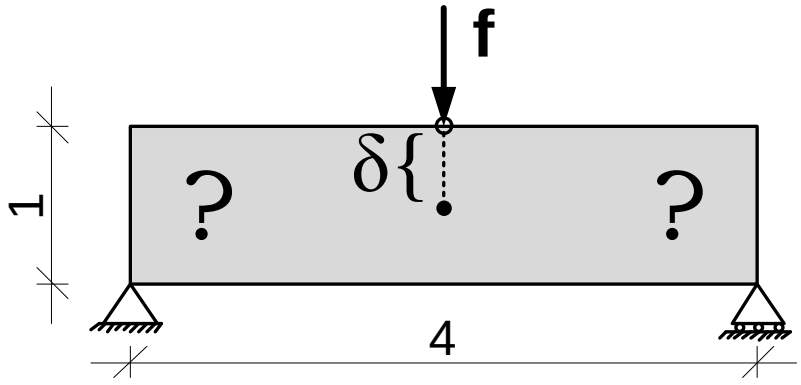

Figure 6: Maximum end-compliance of a simply supported beam: design domain, boundary conditions and prescribed displacement.

The layouts obtained for the simply supported beam resemble actual design of reinforced concrete beams, see Figure 7. Away from the supports, bending action is dominant so steel is necessary in the bottom fibers where tension stresses appear. Closer to the

Table 2: Gradual refinement, example 1

	Design iterations	Penalty factor	Filter radius
$V = 0.1$, stage 1	200	3.0	0.015
$V = 0.1$, stage 2	100	4.0	0.010
$V = 0.2$, stage 1	100	3.0	0.015
$V = 0.2$, stage 2	50	4.0	0.010

supports, shear forces are dominant so concrete typically cracks in an angle of 45°, corresponding to the direction of the principal stresses in pure shear. Consequently, the steel reinforcement should be bent in order to accommodate the tensile stresses due to shear. Additional reinforcement is placed at the upper fibers and at the supports. This is necessary since the load and the reaction forces are concentrated at single nodes. Moreover, the relatively high available volume of steel facilitates the use of steel also in compression, both in the top fibers and in the shear-dominated regions. The reinforcement at the upper fiber can also be interpreted as a means of constraining the curvature due to bending. Therefore steel is preferred there due to its higher Young's modulus so the resulting structure is much stiffer. Comparing the layouts obtained with different volume fractions, it can be seen that the highest priority is given to reinforcement in the bottom fibers that increases the resistance to bending, as well as to reinforcement that essentially stiffens particular regions that bear concentrated forces. When more steel is available, then reinforcement is added to shear-dominated regions as well as to the upper fibers. Concluding this example, the benefit of employing nonlinear modeling is clear when comparing the results to the layout obtained with linear modeling, see Figure 2.

In order to gain more qualitative insight regarding the optimal distribution of reinforcement, we examine an alternative objective function that combines stiffness maximization with minimization of the volume of steel. The volume constraint in (17) is removed and the objective is changed to

$$c = -\left(\beta\theta_N \hat{\mathbf{f}}^T \mathbf{u}_N\right) \times \left(1 - \frac{\sum_{e=1}^{N_e} v_e \rho_e}{\sum_{e=1}^{N_e} v_e}\right)^q \tag{19}$$

where β is a scaling factor (1×10^6 in this case) and the power q varies according to the weight we wish to put on minimizing the volume of steel. Even though the optimized quantity has no physical meaning, examining the optimized designs obtained with this objective can improve our understanding of the priorities in distribution of steel. As we increase the value of q, it is expected that the optimized structure will be less stiff because the utilized amount of steel will decrease. Consequently, reinforcement will be placed only in the regions where it is most necessary. The resulting layouts obtained with this objective are presented in Figure 8 and essentially demonstrate the same priorities as concluded from the designs generated for stiffness maximization with various volume fractions.

Example 2. Beams subject to distributed loads In these example problems, we again address the maximum end-compliance design of beams. We consider more slender

(a) Optimized layout with $V = 0.05$ and $\delta = 0.001$. 200 design iterations with $p_E = 3, p_\alpha = 3, p_{\sigma_y} = 3$ and filter radius $r = 0.015$.

(b) Optimized layout with $V = 0.1$ and $\delta = 0.002$. 300 design iterations with gradual refinement.

(c) Optimized layout with $V = 0.2$ and $\delta = 0.005$. 150 design iterations with gradual refinement.

Figure 7: Maximum end-compliance of a simply supported beam subject to a concentrated load. Black = steel, white = concrete. Layouts obtained for various volume constraints, penalizations and filter radii.

(a) Optimized layout with $q = 1$, 200 design iterations with $p_E = 3, p_\alpha = 3, p_{\sigma_y} = 3$ and filter radius $r = 0.015$.

(b) Optimized layout with $q = 2$, 200 design iterations with $p_E = 3, p_\alpha = 3, p_{\sigma_y} = 3$ and filter radius $r = 0.015$.

(c) Optimized layout with $q = 3$, 200 design iterations with $p_E = 3, p_\alpha = 3, p_{\sigma_y} = 3$ and filter radius $r = 0.015$.

Figure 8: Optimized layouts of a simply supported beam subject to a concentrated load, for the mixed objective (19) with various q values and $\delta = 0.002$. Black = steel, white = concrete.

beams with loads evenly distributed along the length, see Figure 9(a) for the setup of a simply supported beam and Figure 10(a) for the setup of a cantilevered beam. Due to the larger length-to-height ratio, we expect bending action to be much more dominant than in the previous example. The models of the symmetric halves are discretized with 160×40 and 240×40 FE meshes respectively; the volume fraction is set to 0.1 for both cases; and the load is modeled as 10 equally spaced point loads on one half of the beam. For the simply supported beam, we apply a prescribed displacement directed downwards at the mid point of the top fiber, with a magnitude of $\delta = 0.005$. For the cantilevered beam, the prescribed displacement is at the top of the free edge and the magnitude is $\delta = 0.001$. As in the previous example, gradual changes in penalization and filtering are necessary for obtaining the final design, see Table 3 for details.

Table 3: Gradual refinement, example 2

	Design iterations	Penalty factor	Filter radius
Simply supported beam, stage 1	100	3.0	0.040
Simply supported beam, stage 2	50	4.0	0.025
Cantilevered beam, stage 1	200	3.0	0.040
Cantilevered beam, stage 2	100	4.0	0.025

Examining the layouts obtained with distributed loads, it can be seen that the presented procedure enables a clear distinction between tensile and compressive stresses. In the simply supported beam, steel reinforcement is placed in the bottom fiber where tensile stresses appear due to bending, and in the vicinity of concentrated forces (at the supports in this case). Near the supports, the bottom fiber reinforcement is bent upwards. This improves the structure's resistance to shear failure, which is dominant in these regions. In the cantilevered beam, the same principals are followed, so steel is added also to the top fiber above the supports. This reinforcement is bent in both directions according to the varying dominance of shear failure in comparison to bending failure. Finally, it can be observed that small portions of steel are used also to reinforce the support regions and to a lesser extent under loading points.

The case of the simply supported beam was also examined with the mixed objective function (19) and no volume constraint. The resulting layouts are presented in Figure 11. For a relatively low $q = 2$, optimization leads to a very stiff sandwich structure, with the exception that the bottom reinforcement is bent to prevent shear failure. The ability to capture various failure modes demonstrates the strength of the current approach compared to linear elastic modeling. When raising the value of q, the top fiber reinforcement is completely eliminated since it is not essential for the prevention of failure. The designs obtained with $q = 3$ and $q = 4$ are in principal the same as the one generated when constraining the steel volume fraction to be smaller than or equal to 0.1. We again observe bottom-fiber reinforcement that prevents bending failure, which is bent towards the supports to resist shear failure. As in other test cases, some steel is also used as reinforcement in the vicinity of concentrated supports.

Example 3. Short cantilever In this example problem, the proposed procedure is applied for designing the reinforcement in a short cantilever. The design domain is a square

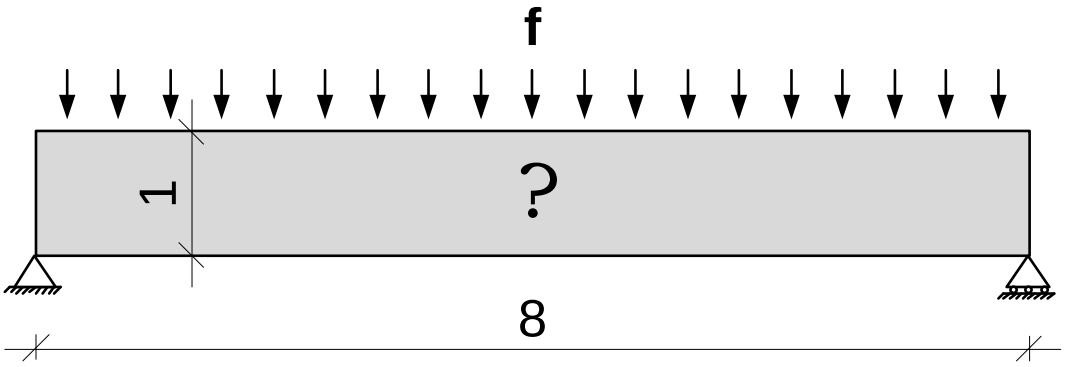

(a) Design domain and boundary conditions.

(b) Optimized layout after 150 design iterations with gradual refinement.

Figure 9: Maximum end-compliance of a simply supported beam subject to a distributed load. Black = steel, white = concrete. Steel consists of 10% of the total volume.

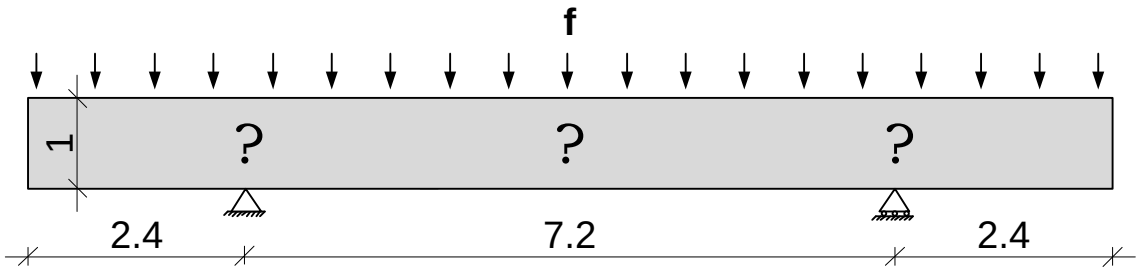

(a) Design domain and boundary conditions.

(b) Optimized layout after 300 design iterations with gradual refinement.

Figure 10: Maximum end-compliance of a cantilevered beam subject to a distributed load. Black = steel, white = concrete. Steel consists of 10% of the total volume.

(a) Optimized layout with $q = 2$, 150 design iterations with gradual refinement.

(b) Optimized layout with $q = 3$, 150 design iterations with gradual refinement.

(c) Optimized layout with $q = 4$, 150 design iterations with gradual refinement.

Figure 11: Optimized layouts of a simply supported beam subject to a distributed load, for the mixed objective (19) with various q values and $\delta = 0.005$. Black = steel, white = concrete.

supported at two corners on one side and loaded with a prescribed displacement directed downwards at the opposite bottom corner, see Figure 12(a). The model is discretized with a 100×100 FE mesh. The objective is to maximize the end-compliance, and we present two results: one of concrete-steel distribution (see (17)) and another of concrete-steel-void distribution (see (18)). For the two-material design, the steel volume fraction is 0.2. When void is considered as well, then the total volume fraction is 0.4 and the steel volume fraction is 0.1. The prescribed displacements are set to $\delta = 0.002$ and $\delta = 0.001$ respectively. The penalty factors are set to the value of 3.0 and the filter radius is $r = 0.015$ for all design iterations.

In both cases, steel is used mainly for a cable-like member in tension, transferring the load to the upper support. This cable is then supported by either a continuous concrete domain (when no voids are possible) or by two compressed concrete bars, see Figures 12(b), 12(c). This again demonstrates the capability of the procedure to distinguish between structural elements in tension and in compression and to choose the appropriate material for each type. The layout obtained when distributing steel, concrete and void resembles strut-and-tie models that are widely used in practical analysis and design of reinforced concrete. As observed in previous examples, steel might be used also for stiffening support regions. In the short cantilever, this is the case mainly for the two material problem with no voids. To a lesser extent, this is observed also in the result of the concrete-steel-void distribution.

Remarks regarding the concrete behavior We note that the presented approach is based on continuum modeling and therefore the structural response mostly resembles a composite continuum. The general tendency is that steel is positioned in regions of major tensile strain, while concrete acts mainly in compression and in mixed stress states. In all the examples presented, the optimized response is in principal very close to linear, with the exception of transition regions where concrete acts together with steel and undergoes

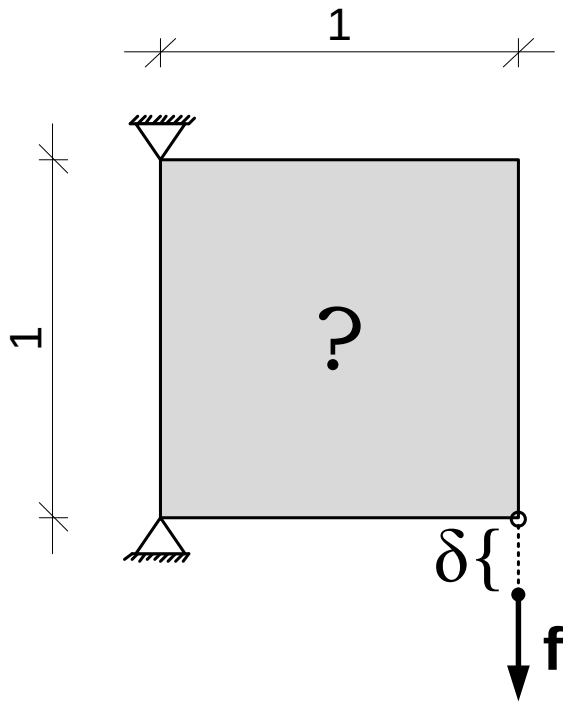

(a) Design domain, boundary conditions and prescribed displacement.

(b) Optimized layout after 500 design iterations, 80% concrete, 20% steel. Black = steel, gray = concrete.

(c) Optimized layout after 200 design iterations, 30% concrete, 10% steel, 60% void. Black = steel, gray = concrete, white = void.

Figure 12: Maximum end-compliance of a short cantilever

tension. Examples are near the ends of the steel bars in the beam problems or in the vicinity of the steel cable in the short cantilever.

Compared to strut-and-tie modeling, this approach offers an alternative means of determining the distribution of tensile reinforcement. Concrete is modeled as elasto-plastic, thus cracking is not considered so the structure remains intact (but with zero stiffness) also after yielding. Nevertheless, when both concrete and steel phases are optimized, the result resembles a strut-and-tie model. This is related to the general tendency in continuum-based topology optimization: material is iteratively added in regions of high principal stresses; ultimately, a truss/frame layout is obtained that is aligned with the principal directions. The same happens in the present formulation that leads to a layout consisting of steel bars in tension and concrete bars in compression, which is in principal the same as one would obtain by a strut-and-tie approach.

6 Discussion

Optimized conceptual design of reinforced concrete was demonstrated, based on a new approach to topology optimization with nonlinear material modeling. The different failure criteria corresponding to the nonlinear response of concrete and steel were taken into account, using material interpolation rules for post-yielding behavior in addition to the standard interpolation of elastic properties. Even though the approach was applied only to the design of steel-reinforced concrete, it can be easily applied to other compositions of materials where it is necessary to capture the nonlinear behavior for the purpose of optimizing the design.

The resulting optimized layouts clearly demonstrate the potential of this approach. When distributing steel within a concrete beam, the placement of reinforcement resembles traditional design and agrees with common engineering knowledge. When distributing concrete, steel and void, the optimized design resembles a strut-and-tie model. The can be used for several purposes: first, to provide the engineer an improved initial design before the detailed design stage; second, to challenge traditional practice and achieve more efficient design of reinforced concrete structures by suggesting non-traditional forms and shapes; third, to reduce weight and concrete production, by utilizing lightweight concrete in the "void" regions where no strength is required.

Future work will focus on more realistic modeling. With respect to loading conditions, it is necessary to consider also self-weight and multiple load cases. Another important issue is the constraint on the volume of reinforcing material: in practice, the relative volume of steel seldom exceeds 1%. This requires either much more refined FE models or other modeling approaches in which thin steel bars can be properly realized. Another important extension is to consider strain softening in the concrete phase. Consequently, transferring tension forces in concrete will be even less preferable, meaning that more realistic designs can be suggested. Finally, the introduction of other objective functions will also be explored.

7 Acknowledgments

The work of the first author was fully funded by the Danish Council for Independent Research - Technology and Production Sciences (FTP - 274-08-0294). This support is gratefully acknowledged. The authors wish to thank Asso. Prof. Mathias Stolpe,

Prof. Ole Sigmund and the two anonymous reviewers for their valuable comments on the manuscript. The authors also thank Prof. Krister Svanberg for allowing them to use the MMA code.

References

[1] O. Amir. *Efficient Reanalysis Procedures in Structural Topology Optimization*. PhD thesis, Technical University of Denmark, 2011.

[2] M. P. Bendsøe. Optimal shape design as a material distribution problem. *Structural Optimization*, 1:193–202, 1989.

[3] M. P. Bendsøe and N. Kikuchi. Generating optimal topologies in structural design using a homogenization method. *Computer Methods in Applied Mechanics and Engineering*, 71:197–224, 1988.

[4] M. P. Bendsøe and O. Sigmund. *Topology Optimization - Theory, Methods and Applications*. Springer, Berlin, 2003.

[5] B. Bourdin. Filters in topology optimization. *International Journal for Numerical Methods in Engineering*, 50:2143–2158, 2001.

[6] M. Bruggi. Generating strut-and-tie patterns for reinforced concrete structures using topology optimization. *Computers and Structures*, 87(23-24):1483–1495, 2009.

[7] T. E. Bruns and D. A. Tortorelli. Topology optimization of non-linear elastic structures and compliant mechanisms. *Computer Methods in Applied Mechanics and Engineering*, 190:3443–3459, 2001.

[8] T. Buhl, C. Pedersen, and O. Sigmund. Stiffness design of geometrically nonlinear structures using topology optimization. *Structural and Multidisciplinary Optimization*, 19(2):93–104, 2000.

[9] W. F. Chen. *Plasticity in Reinforced Concrete*. McGraw-Hill Book Company, New York, 1982.

[10] M. A. Crisfield. *Non-linear Finite Element Analysis of Solids and Structures*, volume 1. John Wiley & Sons, 1991.

[11] D. C. Drucker and W. Prager. Soil mechanics and plastic analysis or limit design. *Quarterly of Applied Mathematics*, 10(2):157–165, 1952.

[12] P. H. Feenstra and R. de Borst. A composite plasticity model for concrete. *International Journal of Solids and Structures*, 33:707–730, 1996.

[13] J. Kato, A. Lipka, and E. Ramm. Multiphase material optimization for fiber reinforced composites with strain softening. *Structural and Multidisciplinary Optimization*, 39(1):63–81, 2009.

[14] H.-G. Kwak and S.-H. Noh. Determination of strut-and-tie models using evolutionary structural optimization. *Engineering Structures*, 28(10):1440–1449, 2006.

[15] Q. Liang, Y. Xie, and G. Steven. Topology optimization of strut-and-tie models in reinforced concrete structures using an evolutionary procedure. *ACI Structural journal*, 97(2):322–330, 2000.

[16] J. Lubliner, J. Oliver, S. Oller, and E. Oñate. A plastic-damage model for concrete. *International Journal of Solids and Structures*, 25:299–326, 1989.

[17] P. Marti. Truss models in detailing. *Concrete International*, 7:66–73, 1985.

[18] K. Maute, S. Schwarz, and E. Ramm. Adaptive topology optimization of elastoplastic structures. *Structural Optimization*, 15(2):81–91, 1998.

[19] P. Michaleris, D. A. Tortorelli, and C. A. Vidal. Tangent operators and design sensitivity formulations for transient non-linear coupled problems with applications to elastoplasticity. *International Journal for Numerical Methods in Engineering*, 37: 2471–2499, 1994.

[20] H. Okamura and M. Ouchi. Self compacting concrete: Development, application and investigations. *journal of Advanced Concrete Technology*, 1:5–15, 2003.

[21] J. Oliver, D. L. Linero, A. E. Huespe, and O. L. Manzoli. Two-dimensional modeling of material failure in reinforced concrete by means of a continuum strong discontinuity approach. *Computer Methods in Applied Mechanics and Engineering*, 197(5):332–348, 2008.

[22] J. Pravida and W. Wunderlich. A plasticity based model and an adaptive algorithm for finite element analysis of reinforced concrete panels. *International Journal for Numerical Methods in Engineering*, 53(11):2445–2462, 2002.

[23] W. Ritter. The hennebique system of construction. *Schweizerische Bauzeitung*, 33/34, 1899.

[24] J. Schlaich, K. Schafer, and M. Jennewein. Toward a consistent design of structural concrete. *PCI journal*, 32(3):74–150, 1987.

[25] O. Sigmund and S. Torquato. Design of materials with extreme thermal expansion using a three-phase topology optimization method. *Journal of the Mechanics and Physics of Solids*, 45(6):1037–1067, 1997.

[26] J. Simo and T. Hughes. *Computational Inelasticity*. Springer, New York, 1998.

[27] H. Stang and M. Geiker. High Performance Concrete. *Arkitekten*, 12:33–35, 2004. (In Danish).

[28] K. Svanberg. The method of moving asymptotes - a new method for structural optimization. *International Journal for Numerical Methods in Engineering*, 24:359–373, 1987.

[29] C. Swan and I. Kosaka. Voigt-Reuss topology optimization for structures with nonlinear material behaviors. *International Journal for Numerical Methods in Engineering*, 40(20):3785–3814, 1997.

[30] O. C. Zienkiewicz and R. L. Taylor. *The Finite Element Method (5th edition) Volume 2 - Solid Mechanics*. Elsevier, 2000.